

# Delta and Omega masses in a three-quark covariant Faddeev approach

Helios Sanchis-Alepuz,<sup>1,\*</sup> Gernot Eichmann,<sup>2</sup> Selym Villalba-Chávez,<sup>1,†</sup> and Reinhard Alkofer<sup>1</sup>

<sup>1</sup>*Institute of Physics, University of Graz, Universitätsplatz 5, 8010, Graz, Austria*

<sup>2</sup>*Institut für Theoretische Physik I, Justus-Liebig-Universität Giessen, D-35392 Giessen, Germany*

(Dated: February 14, 2022)

We present the solution of the Poincaré-covariant Faddeev equation for the  $\Delta(1232)$  and  $\Omega(1672)$  baryons. The covariant structure of the corresponding baryon amplitudes and their decomposition in terms of internal spin and orbital angular momentum is explicitly derived. The interaction kernel is truncated to a rainbow-ladder dressed-gluon exchange such that chiral symmetry and its dynamical breaking are correctly implemented. The resulting physical masses agree reasonably with experiment and their evolution with the pion mass compares favorably with lattice calculations. Evidence for the non-sphericity of the  $\Delta$ -resonance is discussed as well.

PACS numbers: 11.10.St, 12.38.Lg, 14.20.Dh,

## I. INTRODUCTION

Quantum Chromodynamics (QCD) was built upon the understanding of hadrons via the quark model and the discovery of color. However, despite the success of QCD predictions at high energies, which led to the consensus that QCD provides a correct description of strong interactions, the calculation of hadron properties developed at a slower pace. This is due to the fundamental non-perturbative character of bound-state phenomena, and it is further complicated by the low-energy enhancement of strong interactions.

Hadrons, as bound states of quarks and gluons, are described in continuum QCD by (generalized) Bethe-Salpeter equations (BSEs) [1–5] which rely upon the Green functions of the theory. This, in principle, necessitates a solution of the infinite tower of coupled Dyson-Schwinger equations (DSEs) [6–8]. Any feasible numerical procedure thus requires a symmetry-preserving truncation, but once such a truncation is performed, the approach provides a fully consistent quantum-field theoretical framework for the study of hadron properties.

The aforementioned approach has a longstanding and successful history in the investigation of meson properties; see, e.g., [9–11] and references therein. For baryons, however, the relativistic bound-state description is considerably more involved and computationally demanding. The reason is that the presence of a third quark enlarges the momentum phase space, and the relativistic spin structure [12, 13] of the three-quark bound-state amplitude is much more complicated as well. A successful simplification of the problem starts from a covariant Faddeev equation [3, 4] but immediately reduces its complexity by treating the two-body scattering matrix in a separable expansion: by considering quark-quark correlations, called diquarks, as dominant, the three-quark

equation is simplified to a quark-diquark BSE [14–16]. For a collection of recent results using the quark-diquark approach see, e.g., Refs. [17–23].

A step forward was taken in Refs. [13, 24–26] where, for the first time, the full three-body Poincaré-covariant Faddeev equation for the nucleon was solved. Here, the interaction kernel is truncated to a rainbow-ladder dressed-gluon exchange between two of the quarks, and irreducible three-quark contributions are neglected. The nucleon mass reported in these works is comparable to lattice data and, surprisingly, also very close to the quark-diquark result. The calculation has been recently improved in Ref. [27].

In the family of baryon resonances, the  $\Delta(1232)$  isospin quadruplet plays a special role, owing to its high production cross section which makes it one of the best studied resonances. Moreover, it is the lightest baryon resonance and possesses the same valence-quark content as the nucleon, and thus constitutes an excellent system to understand excitations in QCD. It is also the lightest known particle with spin  $3/2$ . At present, due to numerical limitations, such covariant three-body bound-state calculations are performed only for baryons with equal-mass valence quarks. This is the case for the  $\Delta$  quadruplet assuming isospin symmetry. Another spin- $3/2$  ground-state baryon is the  $\Omega(1672)$ : it is a pure strange state and therefore allows to study the quark-mass dependence of  $\Delta$  properties.

In the present work we extend the techniques described in [13, 25, 27] to the case of the  $\Delta$  and  $\Omega$  resonances in view of computing their masses and bound-state amplitudes. We analyze the importance of the different partial-wave contributions and thereby demonstrate that the  $\Delta$  and  $\Omega$  baryons are not pure s-wave states. This represents a first step towards the understanding of baryon deformation from sphericity. A more complete description of baryon structure will require to study the contributions of different internal spin and angular momentum structures to physical observables such as, e.g., electromagnetic form factors or the electromagnetic  $\gamma N \Delta$ -transition.

The paper is organized as follows. In Section II

\* [helios.sanchis-alepuz@uni-graz.at](mailto:helios.sanchis-alepuz@uni-graz.at)

† present address: Max-Planck-Institut für Kernphysik, Saupfercheckweg 1, D-69117 Heidelberg, Germany

we review the Poincaré-covariant Faddeev approach to baryons and the rainbow-ladder truncation of the interaction kernel, and we describe the main features of the covariant decomposition of the Faddeev amplitude for spin-3/2 baryons. In Section III we present our results for the  $\Delta$  and  $\Omega$  masses and compare with lattice data and experimental values. We also discuss the internal angular momentum composition of the amplitudes. Technical details about the partial-wave decomposition and the numerical implementation are described in Appendices A and B, respectively. Our calculations are performed in Euclidean momentum space and Landau gauge QCD; details about the conventions used in this paper can be found, e.g., in Ref. [27].

## II. FADDEEV EQUATION AND RAINBOW-LADDER TRUNCATION

Baryons are described in QCD by the three-quark (six-point) Green function which characterizes the state both on- and off-shell. On the baryon mass shell the Green function has a pole, and a Laurent expansion around this pole allows to derive a relativistic three-body bound-state equation (see Ref. [5] for a pedagogical discussion). That equation reads

$$\Psi = \mathbf{K}_3 G_0^{(3)} \Psi, \quad \mathbf{K}_3 = \mathbf{K}_3^{irr} + \sum_{a=1}^3 \mathbf{K}_{(2)}^{(a)}, \quad (1)$$

where  $\Psi$  represents the baryon's bound-state amplitude and  $G_0^{(3)}$  is the product of three dressed quark propagators. The three-body kernel  $\mathbf{K}_3$  includes all possible correlations among the three quarks: it comprises a three-body irreducible contribution  $\mathbf{K}_3^{irr}$  as well as the sum of the three two-body irreducible interactions with a spectator quark  $a$ ,  $\mathbf{K}_{(2)}^{(a)}$ . The bound-state amplitude  $\Psi$  satisfies

the physical normalization condition

$$\mathcal{N} \bar{\Psi} \left[ \frac{d}{dP^2} \left( \mathbf{K}_3^{-1} - G_0^{(3)} \right) \right] \Psi = 1, \quad (2)$$

where  $\bar{\Psi}$  is the charge-conjugated amplitude and  $P$  the total baryon momentum.

The structure of the bound-state amplitude depends on the baryon of interest. It is the product of color, flavor and spin parts. For spin-1/2 baryons, the spin part is a rank-four Dirac tensor, with three Dirac indices representing the valence quarks and the fourth index the bound state. A spin-3/2 particle is described by a Rarita-Schwinger field so that in this case the spin part of the bound-state amplitude is a mixed tensor with four Dirac indices and one Lorentz index. Moreover, it depends on the three quark momenta  $p_1$ ,  $p_2$  and  $p_3$  which can be conveniently reexpressed in terms of the total momentum  $P$  and two relative momenta  $p$  and  $q$ :

$$\begin{aligned} p &= (1 - \zeta) p_3 - \zeta p_d, & p_1 &= -q - \frac{p}{2} + \frac{1 - \zeta}{2} P, \\ q &= \frac{p_2 - p_1}{2}, & p_2 &= q - \frac{p}{2} + \frac{1 - \zeta}{2} P, \\ P &= p_1 + p_2 + p_3, & p_3 &= p + \zeta P, \end{aligned} \quad (3)$$

where  $p_d = p_1 + p_2$ . The total momentum is constrained by  $P^2 = -M^2$ , with  $M$  being the baryon mass.  $\zeta$  is a free momentum partitioning parameter which we will choose to be  $\zeta = 1/3$ . This choice maximizes the accessible bound-state mass range with respect to the analytic structure of the quark-propagator [24] and also allows for a tremendous simplification of the bound-state equation's solution method (see Appendix B).

The success of the quark-diquark approach to baryon properties supports the idea that quark-quark correlations dominate the binding of baryons. Consequently, we neglect the three-body irreducible contribution  $\mathbf{K}_3^{irr}$ . Then, considering the above discussion about the bound-state amplitude's tensorial structure and kinematics, one arrives at the covariant Faddeev equation for a spin-3/2 baryon (see Fig. 1):

$$\begin{aligned} \Psi_{\alpha\beta\gamma\delta}^\mu(p, q, P) = \int_k & \left[ K_{\beta\beta'\gamma\gamma'}(k) S_{\beta'\beta''}(k_2) S_{\gamma'\gamma''}(\tilde{k}_3) \Psi_{\alpha\beta''\gamma''\delta}^\mu(p^{(1)}, q^{(1)}, P) \right. \\ & + K_{\gamma\gamma'\alpha\alpha'}(k) S_{\gamma'\gamma''}(k_3) S_{\alpha'\alpha''}(\tilde{k}_1) \Psi_{\alpha''\beta\gamma''\delta}^\mu(p^{(2)}, q^{(2)}, P) \\ & \left. + K_{\alpha\alpha'\beta\beta'}(k) S_{\alpha'\alpha''}(k_1) S_{\beta\beta''}(\tilde{k}_2) \Psi_{\alpha''\beta''\gamma\delta}^\mu(p^{(3)}, q^{(3)}, P) \right], \end{aligned} \quad (4)$$

where we have already restricted ourselves to the case where the two-quark kernel depends only on the exchange (i.e., gluon) momentum  $k$ . The quark propagators  $S$  depend on the internal quark momenta  $k_i = p_i - k$  and

$\tilde{k}_i = p_i + k$ . The internal relative momenta are

$$\begin{aligned} p^{(1)} &= p + k, & p^{(2)} &= p - k, & p^{(3)} &= p, \\ q^{(1)} &= q - k/2, & q^{(2)} &= q - k/2, & q^{(3)} &= q + k. \end{aligned} \quad (5)$$

The solution of the Faddeev equation is greatly simpli-

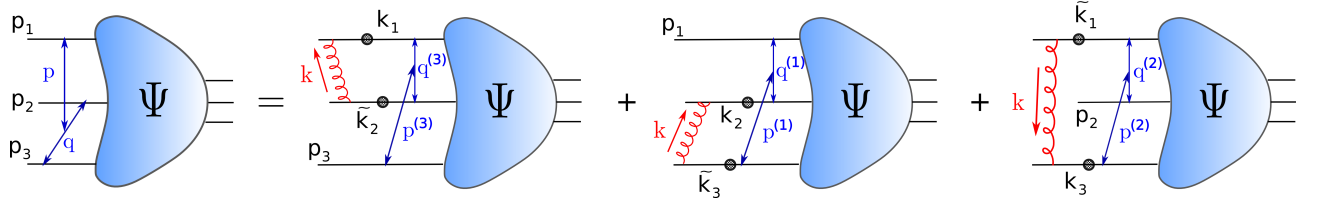


FIG. 1. Diagrammatic representation of the Faddeev equation in rainbow-ladder truncation.

fied if one expresses the Faddeev amplitude in terms of a basis  $\tau_{\alpha\beta\gamma\delta}^i{}^\mu(p, q, P)$ ,

$$\Psi_{\alpha\beta\gamma\delta}^\mu(p, q, P) = \sum_i f_i(p^2, q^2, \{z\}) \tau_{\alpha\beta\gamma\delta}^i{}^\mu(p, q, P), \quad (6)$$

where the expansion coefficients  $f_i$  depend on the five Lorentz-invariant variables

$$p^2, \quad q^2, \quad z_0 = \widehat{p}_T \cdot \widehat{q}_T, \quad z_1 = \widehat{p} \cdot \widehat{P}, \quad z_2 = \widehat{q} \cdot \widehat{P}. \quad (7)$$

Here, a hat denotes a normalized four-vector and the subscript  $T$  a transverse projection with respect to the total momentum  $P$ .

In principle one is free to choose any possible basis  $\tau^i$ . For the sake of physical interpretation it is convenient to perform a partial-wave decomposition and classify the basis elements with respect to their quark-spin and relative orbital angular momentum content in the baryon's rest frame. The explicit derivation of such a basis is quite involved [28] and presented in Appendix A. The most significant aspects of this construction are:

- It is independent of any approximation in the Faddeev equation.
- Only Poincaré covariance as well as parity invariance are needed to construct the basis.
- For positive-parity, positive-energy (particle) spin- $3/2$  baryons the basis consists of 128 elements.
- The basis includes all possible spin and orbital angular momentum values, namely,  $s = 1/2, 3/2$  and  $\ell = 0, 1, 2, 3$ .

Once the Poincaré-covariant structure of the spin- $3/2$  baryon amplitude is determined, the elements in the Faddeev equation that remain to be specified are the two-quark interaction kernel and the quark propagator. They are related by the axial-vector Ward-Takahashi identity (AXWTI) which, in pseudo-scalar meson studies, guarantees the correct implementation of chiral symmetry and its spontaneous breaking. In particular, it implies that pions are massless in the chiral limit [29–35]. The simplest  $qq$  interaction kernel that satisfies the AXWTI is a dressed-gluon ladder exchange:

$$\mathcal{K}_{\alpha\alpha'\beta\beta'}(k) = Z_2^2 \frac{4\pi\alpha(k^2)}{k^2} T_k^{\mu\nu} \gamma_{\alpha\alpha'}^\mu \gamma_{\beta\beta'}^\nu, \quad (8)$$

where  $Z_2$  is the quark renormalization constant,  $T_k^{\mu\nu} = \delta^{\mu\nu} - \hat{k}^\mu \hat{k}^\nu$  is a transverse projector with respect to the gluon momentum  $k$ , and  $\alpha(k^2)$  is an effective interaction that defines the model input.

The quark propagator satisfies the quark Dyson-Schwinger equation whose interaction kernel includes the dressed gluon propagator as well as one bare and one dressed quark-gluon vertex. Consistency with the AXWTI requires to use the same interaction (8) in the quark DSE:

$$S_{\alpha\beta}^{-1}(p) = Z_2 (i\not{p} + m_0)_{\alpha\beta} + \int_q \mathcal{K}_{\alpha\alpha'\beta'\beta}(k) S_{\alpha'\beta'}(q), \quad (9)$$

where  $m_0$  is the bare current-quark mass that enters the equation as an input, and  $k = q - p$ . Tracing the color structure yields a prefactor  $4/3$  in front of the DSE integral in (9) and  $2/3$  for the integral in the Faddeev equation (4). Eqs. (8–9) define the rainbow-ladder truncation where the dressed quark-gluon vertex is truncated to its vector part  $\gamma^\mu$ , and the combined non-perturbative dressing of the gluon propagator and quark-gluon vertex is absorbed in the effective interaction  $\alpha(k^2)$  which has to be modeled.

For the effective coupling we adopt the ansatz introduced in Ref. [36] which has been successfully applied in many hadron studies. It reproduces the logarithmic behaviour of QCD's one-loop running coupling in the ultraviolet, and it is strong enough in the infrared to enable dynamical chiral symmetry breaking and thereby generates a dynamical constituent-quark mass:

$$\alpha(k^2) = \pi\eta^7 \left( \frac{k^2}{\Lambda^2} \right)^2 e^{-\eta^2(k^2/\Lambda^2)} + \alpha_{UV}(k^2). \quad (10)$$

The infrared part is characterized by one dimensionless parameter  $\eta$  and an energy scale  $\Lambda$ . The 'ultraviolet term' reads

$$\alpha_{UV}(k^2) = \frac{2\pi\gamma_m(1 - e^{-k^2/\Lambda_t^2})}{\ln[e^2 - 1 + (1 + k^2/\Lambda_{QCD}^2)^2]}, \quad (11)$$

where  $\gamma_m = 12/(11N_C - 2N_f)$  is the anomalous dimension of the quark propagator. We use  $\gamma_m = 12/25$  and  $\Lambda_{QCD} = 0.234$  GeV. The scale  $\Lambda_t = 1$  GeV is only introduced for technical reasons, its precise value has no impact on the results. The infrared energy scale is fixed to the value  $\Lambda = 0.72$  GeV in order to reproduce the pion

	Nucleon	$\Delta$	$\Omega$
Physical	0.94	1.23	1.67
Q-DQ [23]	0.94	1.28	1.77
Faddeev	0.94 [27]	1.26	1.72

TABLE I. Nucleon,  $\Delta$  and  $\Omega$  masses (in GeV) obtained from the Faddeev equation and, for comparison, in the quark-diquark (Q-DQ) approach [20, 23]. In both cases, the parameter  $\eta$  in Eq. (10) is set to  $\eta = 1.8$ .

decay constant [36]. Many meson observables, and here especially the ones related to ground-state pseudoscalar and vector mesons, turn out to be almost insensitive to the infrared width parameter  $\eta$  around a central value  $\eta = 1.8$  [11], and a similar observation holds for nucleon properties [23, 27].

### III. RESULTS

Having defined the input of the Faddeev equation, Eqs. (4) and (9) can now be solved consistently. The details of the calculation are given in Appendix B. From the solution of the Faddeev equation we obtain the bound-state mass and amplitudes, and the Faddeev amplitudes thereby provide information about the internal structure of the baryon.

For the hadron mass calculation, the current-quark masses must be fixed as well. Upon setting the value for the infrared scale  $\Lambda$ , the  $u/d$  mass is adjusted to reproduce the physical pion mass. Since there is no purely strange pseudoscalar meson, the  $s$ -quark mass is fixed to reproduce the kaon mass which would correspond to a fictitious pseudoscalar  $s\bar{s}$  state  $m_{s\bar{s}} = 690$  MeV.

To analyze the sensitivity of our results to the parameters of the effective interaction, we have repeated our calculations for different values of  $\eta$  in the range 1.6–2.0. For the central value  $\eta = 1.8$ , the resulting  $\Delta$  mass at the physical pion mass, and the  $\Omega$  mass at  $m_\pi = 690$  MeV, are shown in Table I. They are in good agreement with the corresponding experimental values. For comparison, we have also included the respective mass results in the quark-diquark approach [20, 23]. While the same value for the nucleon mass,  $M_N = 0.94$  GeV, is obtained both in the quark-diquark approach and through the Faddeev equation, the quark-diquark results for the spin-3/2 baryon masses are larger. This solidifies the observation that a truncation of the Faddeev kernel to (ground-state) scalar and axial-vector diquark channels is sufficient to reproduce nucleon properties, whereas more structure is needed to describe spin-3/2 baryons. Nevertheless, the results clearly demonstrate that diquarks capture an important part of the internal structure of baryons.

It is interesting to study the relevance of interaction terms beyond the rainbow-ladder truncation. Meson studies show that pionic corrections (pseudoscalar-meson exchange among quarks, so-called resonant corrections)

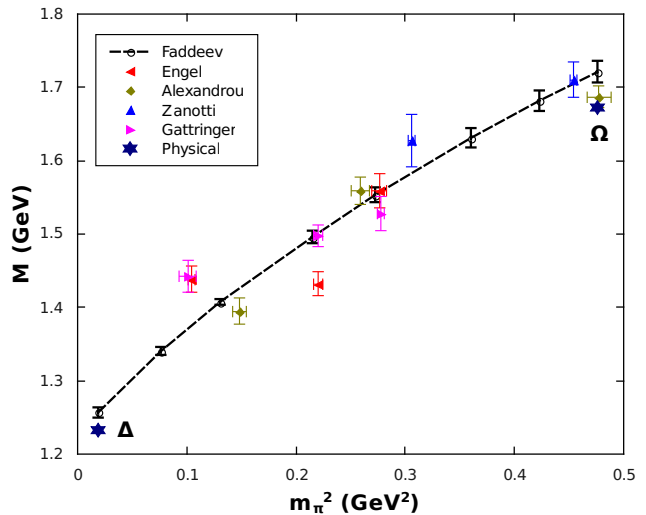


FIG. 2. Evolution of  $M_\Delta$  with  $m_\pi^2$  compared to lattice data [37–40]. Stars denote the experimental values of  $\Delta$  and  $\Omega$ . Error bars in the Faddeev calculation correspond to a variation in the interaction width in the range  $\eta \in 1.6 - 2.0$

are attractive, while non-resonant contributions have a repulsive effect [41–44]. Both effects seem to cancel at the non-perturbative level, so that the rainbow-ladder kernel gives an accurate description of the  $q\bar{q}$  interaction in mesons. Moreover, pionic corrections are expected to be suppressed at high quark masses.

The evolution of the  $\Delta$ -mass with the squared pion mass is shown in Fig. 2 and compared to lattice results. Here, the pion mass is obtained by solving the corresponding Bethe-Salpeter equation using the same interaction kernel upon varying the current-quark mass. We find a good agreement of the Faddeev-calculated masses with lattice data, especially at higher pion masses. If the analysis of meson results for effects beyond rainbow-ladder can be extended to the  $qq$ -interaction in baryons, this would indicate that a near cancelation of resonant and non-resonant contributions prevails up to the strange-quark mass and beyond.

Ultimately, such issues can only be clarified by overcoming the rainbow-ladder truncation as well as the restriction to quark-quark correlations in the Faddeev equation. We note, however, that the current-mass evolution of the  $\Delta$  mass from the Faddeev equation is in qualitative agreement with that of the vector-meson mass obtained from its Bethe-Salpeter equation, cf. Fig. 2 in Ref. [23]. Using the current-mass independent interaction defined in Eq. (10), both resulting curves overestimate the experimental values of  $M_\Omega$  and  $m_\Phi$  at the strange-quark mass approximately by the same amount ( $\sim 3\%$ ). In view of this, it could be misleading to attribute such discrepancies solely to corrections beyond rainbow-ladder without understanding the sensitivity of our calculations to the effective interaction  $\alpha(k^2)$ . It



would be desirable to compare results using different, lattice-inspired, model interactions; see also Ref. [45]. Such a study will be published elsewhere.

There is another missing feature in the current-mass evolution of the  $\Delta$  mass. The  $\Delta$  resonance can decay into a nucleon via the emission of a pion. Such a decay would manifest itself in a non-analytical behaviour of the  $\Delta$  mass as a function of the pion mass when the decay channel opens, *i.e.* for  $m_\pi \sim M_\Delta - M_N \sim 300$  MeV [46, 47]. Our truncation scheme does not provide a mechanism for the  $\Delta$  to decay and thus we should obtain a higher  $\Delta$  mass, shifted approximately 100 MeV upwards, corresponding to the  $\Delta$  decay width. Again, an analogous observation holds for the  $\rho$ -meson obtained through the Bethe-Salpeter equation [23, 36]. Therefore, we conclude that the model provides too much binding in the light pion-mass region where the decay channel would be opened in a full calculation.

A first hint on the internal structure of the  $\Delta$ -baryon comes from the analysis of the relative importance of the different quark-spin and relative angular-momentum contributions. In Fig. 3 we plot the dominant amplitudes in each partial-wave sector (see Appendix A). It is clear that the  $s = 3/2, \ell = 0$  (*i.e.*, s-wave) sector is dominant. However, p- and d-wave sectors are much larger in number of basis elements, thus even small values of individual basis elements can add up to a non-negligible contribution of a given sector and thereby cause deviations from sphericity. We obtain very similar results for the  $\Omega$ -baryon. In any case, a thorough understanding of the  $\Delta$  and  $\Omega$  internal structure requires the study of the different partial-wave sectors in physical observables, *e.g.*, form factors.

#### IV. CONCLUSIONS

We presented a fully Poincaré-covariant solution of the Faddeev equation for the  $\Delta$ - and  $\Omega$ -baryons. The required quark propagators are obtained by consistently solving the corresponding Dyson-Schwinger equations. For this we employed a rainbow-ladder truncation of the interaction kernel, dressed by an effective interaction which effectively depends on a single parameter and is fixed to reproduce the pion decay constant.

We obtain masses that are in good agreement with experimental results and their evolution with the pion mass compares favorably with lattice results. We concluded, however, that the effective interaction we used provides too much binding in the low pion-mass region.

The contribution of the different quark-spin and relative orbital angular momentum sectors was studied by naïvely comparing the magnitude of the corresponding dominant amplitudes. This shows an s-wave dominance, however with a non-negligible p- and d-wave contribution. A better understanding of the internal structure would come from the study of  $\Delta$  and  $\Omega$  form factors in the present framework. Work in this direction is in progress.

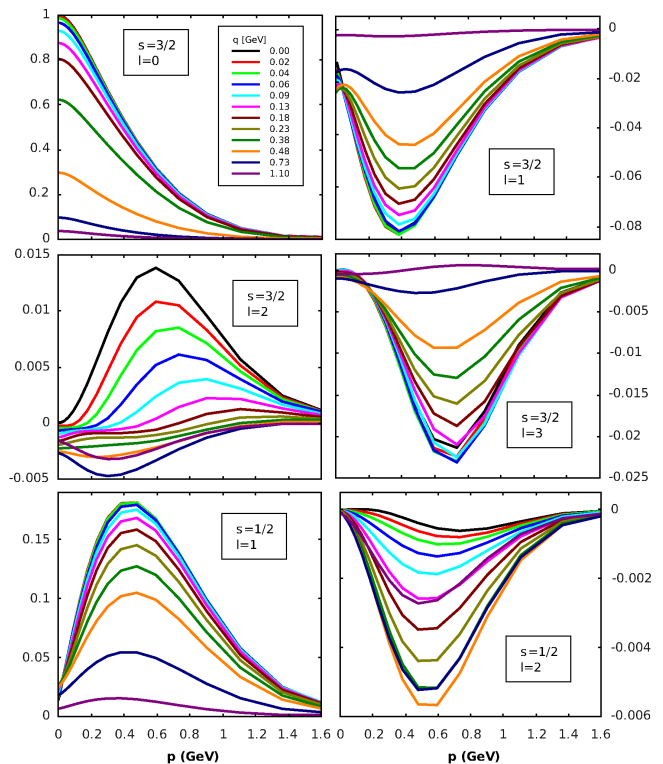


FIG. 3. Zeroth Chebyshev moments of the coefficients  $f_i$  in the basis expansion of Tables II and III. We plot the coefficients dominant in each  $(s, \ell)$ -sectors as a function of  $p$  and  $q$ . The normalization is chosen such that  $f_1(p^2 = 0, q^2 = 0) = 1$ . The respective basis elements  $\tau_{ij}^{\sigma, k}$  are from left to right, top to bottom:  $\tau_{11}^{+1}, \tau_{13}^{+1}, \tau_{22}^{-2}, \tau_{33}^{-1}, \tau_{63}^{+1}, \tau_{74}^{+2}$ .

#### Acknowledgments

We are grateful to M. Blank, C.S. Fischer, A. Krassnigg, D. Nicmorus and R. Williams for helpful discussions. This work was supported by the Austrian Science Fund FWF under Projects No. P20592-N16, Erwin-Schrödinger-Stipendium J3039, and the Doctoral Program W1203; by the Helmholtz International Center for FAIR within the LOEWE program of the State of Hesse; as well as in part by the European Union (Hadron-Physics2 project “Study of strongly-interacting matter”).

#### Appendix A: Covariant decomposition of the $\Delta$ -baryon amplitude

The spin part of the Faddeev amplitude for spin-3/2 particles is a mixed tensor with four Dirac indices and one Lorentz index. The positive-parity and positive-energy subspace can be expanded in a basis with 128 elements  $\tau_{\alpha\beta\gamma\delta}^i{}^\mu(p, q, P)$ , cf. Eq. (6), which can be classified with

$s$	$\ell$	$\sqrt{5} \tau_{1j}^{\sigma,1}$
$3/2$	$0$	$\sqrt{5} S_{11}^g$
$3/2$	$1$	$3 S_{12}^g + 2 (V_{14}^r - V_{13}^s)$
$3/2$	$1$	$3 S_{13}^g + 2 V_{11}^r$
$3/2$	$1$	$3 S_{14}^g + 2 V_{11}^s$
$s$	$\ell$	$\frac{1}{\sqrt{3}} \tau_{2j}^{\sigma,1}$
$3/2$	$2$	$S_{11}^g + S_{31}^r + 2 S_{41}^s - \frac{1}{3} (V_{13}^r + 2 V_{14}^s)$
$3/2$	$2$	$S_{12}^g - 2 S_{41}^r - \frac{2}{3} (V_{13}^s - 2 V_{14}^r)$
$3/2$	$2$	$S_{13}^g + 2 (S_{43}^s - S_{34}^s) + \frac{2}{3} (V_{11}^r + 2 V_{12}^s)$
$3/2$	$2$	$S_{14}^g - 2 (S_{43}^r - S_{34}^r) + \frac{2}{3} (V_{11}^s - 2 V_{12}^r)$
$s$	$\ell$	$\sqrt{5} \tau_{3j}^{\sigma,1}$
$3/2$	$2$	$\sqrt{5} (S_{11}^g + 3 S_{31}^r - V_{13}^r)$
$3/2$	$3$	$4 S_{12}^g + 5 (S_{32}^r + S_{42}^s) + V_{14}^r - V_{13}^s$
$3/2$	$3$	$S_{13}^g + 5 S_{33}^r - V_{11}^r$
$3/2$	$3$	$S_{14}^g + 5 S_{44}^s - V_{11}^s$
$s$	$\ell$	$\frac{1}{\sqrt{3}} \tau_{4j}^{\sigma,1}$
$3/2$	$3$	$S_{11}^g + 2 (S_{32}^s + S_{41}^s + S_{31}^r) - \frac{2}{3} (V_{13}^r + 2 V_{14}^s)$
$3/2$	$3$	$S_{32}^r - S_{42}^s - \frac{1}{3} (V_{13}^s + V_{14}^r)$
$3/2$	$3$	$S_{13}^g + S_{33}^r + 2 S_{43}^s + \frac{1}{3} (V_{11}^r + 2 V_{12}^s)$
$3/2$	$3$	$S_{14}^g + S_{44}^s + 2 S_{34}^r + \frac{1}{3} (V_{11}^s - 2 V_{12}^r)$

TABLE II. Orthonormal Dirac basis  $\tau_{ij}^{\sigma,k}$  for  $s = 3/2$  and  $k = 1$ . We omit Dirac and Lorentz indices as well as the label  $\sigma = \pm$  for better readability. The dominant covariants in each  $(s, \ell)$ -sector which are plotted in Fig. 3 are highlighted; the relevant values of  $\sigma$  and  $k$  are given in the caption of Fig. 3.

respect to their quark-spin and relative orbital angular momentum in the baryon's rest frame. The resulting basis is collected in Tables II and III, and in the following we will sketch its derivation.

To begin with, it is convenient to express the momenta  $\{p, q, P\}$  that enter the basis elements through orthogonal unit vectors  $\{r, s, \hat{P}\}$  which satisfy  $r^2 = s^2 = \hat{P}^2 = 1$  and  $r \cdot s = r \cdot \hat{P} = s \cdot \hat{P} = 0$ . This is achieved by taking the component of  $p$  transverse to  $P$ , and by projecting  $q$  onto the direction transverse to  $P$  and  $r$ :

$$r := \widehat{p_T} = \frac{\hat{p} - z_1 \hat{P}}{\sqrt{1 - z_1^2}}, \quad \widehat{q_T} = \frac{\hat{q} - z_2 \hat{P}}{\sqrt{1 - z_2^2}}, \quad s := \frac{\widehat{q_T} - z_0 r}{\sqrt{1 - z_0^2}}$$

with the Lorentz-invariant momentum variables  $z_1, z_2$  and  $z_0$  from Eq. (7). In the baryon's rest frame and a suitable choice of coordinates,  $r, s$  and  $\hat{P}$  become the Euclidean unit vectors  $e_3, e_2$  and  $e_4$ .

$s$	$\ell$	$\frac{1}{\sqrt{3}} \tau_{5j}^{\sigma,1}$	$\tau_{6j}^{\sigma,1}$
$1/2$	$2$	$S_{13}^r + S_{14}^s$	$V_{13}^r + V_{14}^s$
$1/2$	$1$	$S_{14}^r - S_{13}^s$	$V_{14}^r - V_{13}^s$
$1/2$	$1$	$S_{11}^r$	$V_{11}^r$
$1/2$	$1$	$S_{11}^s$	$V_{11}^s$
$s$	$\ell$	$\tau_{7j}^{\sigma,1}$	$\sqrt{3} \tau_{8j}^{\sigma,1}$
$1/2$	$2$	$S_{13}^r - S_{14}^s$	$V_{13}^r - V_{14}^s$
$1/2$	$2$	$S_{13}^s + S_{14}^r$	$V_{13}^s + V_{14}^r$
$1/2$	$2$	$S_{11}^r + 2 S_{12}^s$	$V_{11}^r + 2 V_{12}^s$
$1/2$	$2$	$S_{11}^s - 2 S_{12}^r$	$V_{11}^s - 2 V_{12}^r$

TABLE III. Orthonormal Dirac basis  $\tau_{ij}^{\sigma,k}$  for  $s = 1/2$  and  $k = 1$ . We omit Dirac/Lorentz indices and the label  $\sigma$ . The dominant covariants in each  $(s, \ell)$ -sector are highlighted.

Next, we define the basic Dirac structures

$$\Gamma_{i=1\dots 4} = \{\mathbb{1}, \not{r}, \not{s}, \not{\hat{P}}\} \quad (\text{A1})$$

which we use to construct a (still linearly dependent) basis for a rank-four Dirac tensor:

$$\begin{pmatrix} S_{ij}^\sigma \\ P_{ij}^\sigma \\ V_{ij}^\sigma \\ A_{ij}^\sigma \end{pmatrix} := \begin{pmatrix} \mathbb{1} \otimes \mathbb{1} \\ \gamma^5 \otimes \gamma^5 \\ \gamma_T^\mu \otimes \gamma_T^\mu \\ \gamma_T^\mu \gamma^5 \otimes \gamma_T^\mu \gamma^5 \end{pmatrix} (\Gamma_i \otimes \Gamma_j) \Omega^\sigma(\hat{P}). \quad (\text{A2})$$

Here,  $\gamma_T^\mu$  is the  $\gamma$ -matrix transverse to  $P$ , and we used  $\Omega^\pm(\hat{P}) = \Lambda^\pm(\hat{P}) \gamma^5 \mathcal{C} \otimes \Lambda^\pm(\hat{P})$ , where  $\mathcal{C} = \gamma^4 \gamma^2$  is the charge conjugation-matrix and  $\Lambda^\pm(\hat{P}) = (\mathbb{1} \pm \hat{P})/2$  are the positive- and negative-energy projectors. The tensor products are understood as

$$(f \otimes g)_{\alpha\beta\gamma\delta} = f_{\alpha\beta} g_{\gamma\delta}, \quad (f_1 \otimes f_2)(g_1 \otimes g_2) = (f_1 g_1) \otimes (f_2 g_2). \quad (\text{A3})$$

Denoting the elements in Eq. (A2) generically by  $M_{ij}^\sigma$ , with  $M \in \{S, P, V, A\}$  and  $i, j = 1 \dots 4$ , we can construct the building blocks of a Dirac-Lorentz basis for the  $\Delta$ -baryon in the following way:

$$\begin{pmatrix} [M_{ij}^g]^{\sigma,\nu} \\ [M_{ij}^r]^{\sigma,\nu} \\ [M_{ij}^s]^{\sigma,\nu} \end{pmatrix} := \begin{pmatrix} \gamma_T^\mu \gamma^5 \otimes \mathbb{1} \\ r^\mu \gamma^5 \otimes \mathbb{1} \\ s^\mu \gamma^5 \otimes \mathbb{1} \end{pmatrix} (M_{ij}^\sigma) (\mathbb{1} \otimes \mathbb{P}^{\mu\nu}), \quad (\text{A4})$$

where  $\mathbb{P}^{\mu\nu}$  is the Rarita-Schwinger projector for positive-energy particles:

$$\mathbb{P}_+^{\mu\nu}(\hat{P}) = \Lambda^+(\hat{P}) \left( T_P^{\mu\nu} - \frac{1}{3} \gamma_T^\mu \gamma_T^\nu \right). \quad (\text{A5})$$

The set (A4) contains 384 elements, but one can show that only 128 of them are linearly independent. We found the following choice of linearly independent elements convenient:

$$\left\{ \begin{array}{l} S_{1j}^r, S_{1j}^s \\ P_{1j}^r, P_{1j}^s \\ V_{1j}^r, V_{1j}^s \\ A_{1j}^r, A_{1j}^s \end{array} \right\}, \quad \left\{ \begin{array}{l} S_{43}^r, S_{41}^r \\ S_{32}^s, S_{34}^s \\ P_{43}^r, P_{41}^r \\ P_{32}^s, P_{34}^s \end{array} \right\}, \quad (A6)$$

$$\left\{ \begin{array}{l} S_{1j}^g \\ P_{1j}^g \end{array} \right\}, \quad \left\{ \begin{array}{l} S_{3j}^r, S_{4j}^s \\ P_{3j}^r, P_{4j}^s \end{array} \right\},$$

with  $j = 1 \dots 4$ , and we have omitted the index  $\sigma$  for better readability. The set (A6) includes the element

$$[S_{11}^g]^{\sigma,\nu} = (\gamma_T^\mu \gamma^5 \otimes \mathbb{1}) \Omega^\sigma(\hat{P}) (\mathbb{1} \otimes \mathbb{P}^{\mu\nu}) = \Lambda^\sigma(\hat{P}) \gamma_T^\mu \mathcal{C} \otimes \mathbb{P}^{\mu\nu} \quad (A7)$$

which is familiar from the quark-diquark model and represents the dominant  $s$ -wave structure in the  $\Delta$ -baryon amplitude.

Let us now turn to the partial-wave analysis of these basis elements. In the baryon rest frame, the quark total spin and relative angular momentum operators read

$$S^2 = \frac{9}{4} (\mathbb{1} \otimes \mathbb{1} \otimes \mathbb{1}) + \frac{1}{2} (\sigma_T^{\mu\nu} \otimes \sigma_T^{\mu\nu} \otimes \mathbb{1} + \text{perm.}),$$

$$L^2 = L_{(p)}^2 + L_{(q)}^2 + 2 L_{(p)} \cdot L_{(q)}, \quad (A8)$$

where  $\sigma_T^{\mu\nu} = -\frac{i}{2} [\gamma_T^\mu, \gamma_T^\nu]$  and

$$\begin{aligned} L_{(p)}^2 &= 2 \mathbf{p} \cdot \nabla_{\mathbf{p}} + p^i (\mathbf{p} \cdot \nabla_{\mathbf{p}}) \nabla_{\mathbf{p}}^i - \mathbf{p}^2 \Delta_{\mathbf{p}}, \\ L_{(q)}^2 &= 2 \mathbf{q} \cdot \nabla_{\mathbf{q}} + q^i (\mathbf{q} \cdot \nabla_{\mathbf{q}}) \nabla_{\mathbf{q}}^i - \mathbf{q}^2 \Delta_{\mathbf{q}}, \\ L_{(p)} \cdot L_{(q)} &= p^i (\mathbf{q} \cdot \nabla_{\mathbf{p}}) \nabla_{\mathbf{q}}^i - (\mathbf{p} \cdot \mathbf{q}) (\nabla_{\mathbf{p}} \cdot \nabla_{\mathbf{q}}), \end{aligned} \quad (A9)$$

and  $\mathbf{p}, \mathbf{q}$  are the spatial parts of  $p_T$  and  $q_T$ , respectively.

It is useful to realize that the basis elements containing  $\{S, V\}$  and  $\{P, A\}$ , which differ by a factor  $\gamma^5 \otimes \gamma^5$ , and those with a different value for the index  $\sigma = \pm$ , do not mix under the action of  $S^2$  or  $L^2$  and thus can be analyzed independently. Moreover, from Eqs. (A8) and (A9) one infers that the set (A6) can be further subdivided into four subsets which, due to their different momentum dependence, again do not mix under  $S^2$  or  $L^2$ :

$$\begin{aligned} 1, r^2, s^2, r^2 s^2 : & S_{11}^g, S_{13}^r, S_{14}^s, S_{31}^r, S_{41}^s, S_{32}^s, V_{13}^r, V_{14}^s \\ rs, r^3 s, r s^3 : & S_{12}^g, S_{14}^r, S_{13}^s, S_{42}^s, S_{41}^r, S_{32}^r, V_{14}^r, V_{13}^s \\ r, r s^2, r^3 : & S_{13}^g, S_{11}^r, S_{12}^s, S_{33}^r, S_{34}^s, S_{43}^s, V_{11}^r, V_{12}^s \\ s, r^2 s, s^3 : & S_{14}^g, S_{12}^r, S_{11}^s, S_{44}^s, S_{34}^r, S_{43}^r, V_{12}^r, V_{11}^s \end{aligned}$$

Here, the left column symbolically indicates the different momentum dependencies of the basis elements in powers of  $r$  and  $s$ . The partial-wave analysis is now considerably simplified since we only need to look for eigenfunctions of  $S^2$  and  $L^2$  within the above subsets.

The operator  $S^2$  is independent of the momentum content of the basis elements. Therefore it is sufficient to find the eigenstates at fixed values for the unit vectors  $r$  and  $s$ . At this point the problem can be easily implemented and solved using a symbolic programming language. Similarly, the orbital angular-momentum decomposition can be done straightforwardly on a computer, but it is nevertheless instructive to study some simple examples. The  $\ell = 0$  elements can be found immediately: they are the momentum-independent elements in (A6), i.e.,  $[S_{11}^g]^\sigma$  and  $[P_{11}^g]^\sigma$ . The remaining basis elements can be written as contractions of

$$r^\alpha, s^\alpha, r^\alpha s^\beta, r^\alpha r^\beta, s^\alpha s^\beta, r^\alpha r^\beta s^\delta, \dots \quad (A10)$$

with appropriate momentum-independent Dirac-Lorentz tensors. For the  $\ell = 1$  elements it is sufficient to consider the first three elements in the list above. Applying the orbital angular-momentum operator yields

$$\begin{aligned} L^2 r^\alpha &= 2 r^\alpha, \\ L^2 s^\alpha &= 2 s^\alpha, \\ L^2 r^\alpha s^\beta &= 4 r^\alpha s^\beta + 2 s^\alpha r^\beta, \end{aligned} \quad (A11)$$

and thus the  $\ell = 1$  eigenfunctions are given by:

$$r^\alpha, s^\alpha, r^\alpha s^\beta - s^\alpha r^\beta. \quad (A12)$$

Their contraction with the corresponding Dirac-Lorentz structures yields the  $\ell = 1$  eigentensors at the level of the basis elements. For other  $\ell$  values the calculation proceeds along the same lines but is more involved.

The above analysis focused on the subset  $\{S, V\}$ , which we denote by the index  $k = 1$ . The final result of the partial-wave decomposition for  $k = 1$  is presented in Tables II and III. Analogous results hold for the set  $\{P, A\}$ , denoted by  $k=2$ : the respective basis elements are obtained by exchanging  $S \rightarrow P$ ,  $V \rightarrow A$  and adding an extra minus sign to the elements  $P_{1j}^g$ . For the compilation in Tables (II–III), the original label  $i = 1 \dots 128$  that appears in Eq. (6) was dissolved into the indices  $i = 1 \dots 8$ ,  $j = 1 \dots 4$ ,  $k = 1, 2$ , and  $\sigma = \pm$ .

The resulting basis satisfies the following orthonormality relation:

$$\begin{aligned} \frac{1}{8} \text{Tr} \left\{ \bar{\tau}_{ij}^{\sigma,k} \tau_{i'j'}^{\sigma',k'} \right\} &= \frac{1}{8} [\bar{\tau}_{ij}^{\sigma,k}]_{\beta\alpha\delta\gamma}^\mu [\tau_{i'j'}^{\sigma',k'}]_{\alpha\beta\gamma\delta}^\mu = \\ &= \delta_{ii'} \delta_{jj'} \delta_{kk'} \delta_{\sigma\sigma'}, \end{aligned} \quad (A13)$$

where the conjugation of the basis elements is defined as

$$\begin{aligned} \bar{\tau}_{\alpha\beta\gamma\delta}^\mu(p, q, P) &= \\ -C_{\alpha\alpha'} C_{\gamma\gamma'} \tau_{\beta'\alpha'\delta'\gamma'}^\mu(-p, -q, -P) C_{\beta'\beta}^T C_{\delta'\delta}^T. \end{aligned} \quad (A14)$$

## Appendix B: Numerical details

The numerical techniques used in this work are an extension of those explained in Ref. [27] towards the case

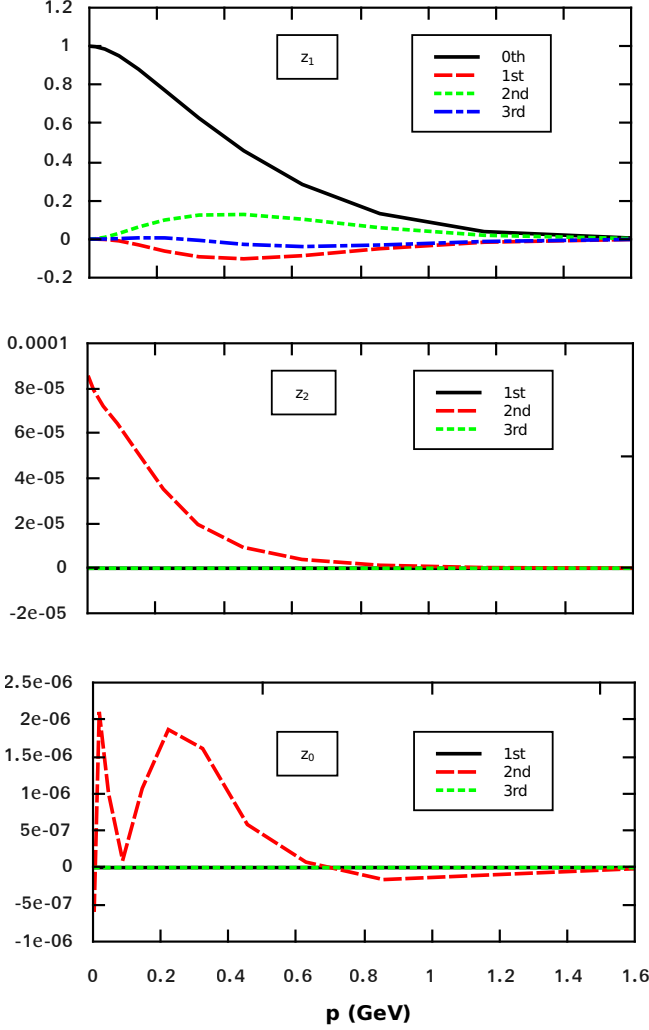


FIG. 4. First four Chebyshev moments in the variables  $z_0$ ,  $z_1$  and  $z_2$  for the dominant amplitude  $[S_{11}^g]^+$  at  $q^2 = 0$ . Note that the zeroth order is the same for all three figures; in the lower two panels it is not shown for clarity.

of the  $\Delta$ -baryon. We summarize the main ideas in this appendix.

The Faddeev amplitude is the product of color, flavor and spin parts. As required by the Pauli principle, that product must be antisymmetric under the exchange of any two of the three quarks. Since a baryon is a color singlet, the color part of the Faddeev amplitude is always antisymmetric, and thus the product of flavor and spin parts must be symmetric. This symmetry requirement allows to relate the three diagrams in Fig. 1.

Compared to the nucleon, the situation is simpler for the  $\Delta$ - and  $\Omega$ -baryons. Since the  $\Delta$  carries isospin  $3/2$ , its flavor part is completely symmetric and hence also the spin part must be symmetric. The  $\Omega$ , on the other hand, is a pure s-quark state and thus automatically symmetric in flavor space. Using this, and starting from Eq. (4), it

is not difficult to show that the first two terms in the equation can be reexpressed in terms of the third one, evaluated at different momenta:

$$\begin{aligned} \Psi_{\alpha\beta\gamma\delta}^{(3)\mu}(p, q, P) = & \Psi_{\alpha\beta\gamma\delta}^{(3)\mu}(p, q, P) \\ & + \Psi_{\beta\gamma\alpha\delta}^{(3)\mu}(p', q', P) \\ & + \Psi_{\gamma\alpha\beta\delta}^{(3)\mu}(p'', q'', P), \end{aligned} \quad (\text{B1})$$

where the permuted relative momenta are given by

$$\begin{aligned} p' &= -q - \frac{p}{2}, & q' &= -\frac{q}{2} + \frac{3p}{4}, \\ p'' &= q - \frac{p}{2}, & q'' &= -\frac{q}{2} - \frac{3p}{4}. \end{aligned} \quad (\text{B2})$$

In terms of the amplitude decomposition (6), the Faddeev equation is written as

$$f_i(p, q, P) = \sum_{a=1}^3 f_i^{(a)}(p, q, P), \quad (\text{B3})$$

where we used the notation

$$\begin{aligned} f_i^{(a)}(p, q, P) &= \int_k \mathcal{K}_{ij}^{(a)}(p, q, P; k) \phi_j^{(a)}(p^{(a)}, q^{(a)}, P), \\ \phi_i^{(a)}(p, q, P) &= \mathcal{G}_{ij}^{(a)}(p, q, P) f_j(p, q, P), \end{aligned} \quad (\text{B4})$$

with  $p^{(a)}$  and  $q^{(a)}$  being the internal relative momenta from Eq. (5). The functions  $\phi_i^{(a)}$  are the coefficients of the so-called wave functions  $\Phi^{(a)} = S(p_b)S(p_c)\Psi$  in the basis expansion (6), where  $\{a, b, c\}$  is a symmetric permutation of  $\{1, 2, 3\}$ , and  $\mathcal{K}_{ij}$  and  $\mathcal{G}_{ij}$  are the matrix representations of the kernel and propagator operators in that basis. Eq. (B1) can be written in terms of the coefficients  $f_i(p, q, P)$  as

$$\begin{aligned} f_i(p, q, P) = & f_i^{(3)}(p, q, P) \\ & + H'_{ij} f_j^{(3)}(p', q', P) \\ & + H''_{ij} f_j^{(3)}(p'', q'', P), \end{aligned} \quad (\text{B5})$$

where the matrices  $H'$  and  $H''$  are defined by

$$\begin{aligned} H'_{ij}(p, q, P) &= \frac{1}{8} \bar{\tau}_{\beta\alpha\delta\gamma}^i \tau_{\beta\gamma\alpha\delta}^j \mu(p, q, P) \tau_{\beta\gamma\alpha\delta}^j \mu(p', q', P), \\ H''_{ij}(p, q, P) &= \frac{1}{8} \bar{\tau}_{\beta\alpha\delta\gamma}^i \tau_{\beta\alpha\delta\gamma}^j \mu(p, q, P) \tau_{\gamma\alpha\beta\delta}^j \mu(p'', q'', P). \end{aligned} \quad (\text{B6})$$

In rewriting the equation we have used the orthogonality (A13) of the basis.

The algorithm for solving the Faddeev equation begins by introducing a fictitious eigenvalue  $\lambda(M)$  in front of the integral in (B4). The integral equation is then solved by iteration: start with a guess for the bound-state mass  $M$  and the initial amplitudes  $f_i$ ; compute the integral (B4) for the case  $a = 3$ ; apply the permutation (B5); and repeat until the eigenvalue  $\lambda(M)$  has converged. If the



converged value is  $\lambda(M) = 1$ , then  $M$  is the correct mass for the bound state; otherwise one has to change the guess for  $M$  and repeat the procedure.

For the presented solutions of the Faddeev equation we expanded the angular dependence of the Faddeev amplitudes in terms of Chebyshev polynomials. This is convenient because only a small number of Chebyshev moments are needed, as shown in Fig. 4.

Solving the Faddeev equation in the form (B4–B5) is a great simplification with respect to the original formulation (4) since the kernel matrix  $\mathcal{K}^{(3)}$  is comparatively simpler than the other two permuted kernels. Note that in this case the external and internal relative momenta  $p$  and  $p^{(3)}$  are the same, cf. Eq. (5). If one uses a moder-

ate number of integration points, and taking into account the fact that the kernel matrices are typically sparse, then the kernel matrix can be computed and stored in advance which notably reduces the computing time. However, if the number of integration points is increased, memory limitations become an issue. For the presented results we have used the following number of integration points: 20 for  $\{p^2, q^2, k^2\}$ , 8 for  $z_0$  and 4 for  $\{z_1, z_2, z, y\}$ . For this configuration, and without storing the kernel matrix in advance (although it would be feasible), each iteration requires approximately four CPU-hours on a 16-node 2.66 GHz cluster, and convergence for  $\lambda(M)$  is usually reached within 15–20 iterations.

- 
- [1] E. E. Salpeter and H. A. Bethe, *Phys. Rev.* **84**, 1232 (1951).
  - [2] L. D. Faddeev, *Sov. Phys. JETP* **12**, 1014 (1961), [*Zh. Eksp. Teor. Fiz.* **39**, 1014 (1960)].
  - [3] J. G. Taylor, *Phys. Rev.* **150**, 1321 (1966).
  - [4] M. Boehm and R. F. Meyer, *Annals Phys.* **120**, 360 (1979).
  - [5] U. Loring, K. Kretzschmar, B. C. Metsch, and H. R. Petry, *Eur. Phys. J.* **A10**, 309 (2001).
  - [6] R. Alkofer and L. von Smekal, *Phys. Rept.* **353**, 281 (2001).
  - [7] C. S. Fischer, *J. Phys.* **G32**, R253 (2006).
  - [8] L. Chang, C. D. Roberts, and P. C. Tandy, 1107.4003 [*nucl-th*].
  - [9] P. Maris and P. C. Tandy, *Nucl. Phys. Proc. Suppl.* **161**, 136 (2006).
  - [10] P. Maris, *AIP Conf. Proc.* **892**, 65 (2007).
  - [11] A. Krassnigg, *Phys. Rev.* **D80**, 114010 (2009).
  - [12] C. Carimalo, *J. Math. Phys.* **34**, 4930 (1993).
  - [13] G. Eichmann, R. Alkofer, A. Krassnigg, and D. Nicmorus, *EPJ Web Conf.* **3**, 03028 (2010).
  - [14] G. Hellstern, R. Alkofer, M. Oettel, and H. Reinhardt, *Nucl. Phys.* **A627**, 679 (1997).
  - [15] M. Oettel, G. Hellstern, R. Alkofer, and H. Reinhardt, *Phys. Rev.* **C58**, 2459 (1998).
  - [16] J. C. R. Bloch, C. D. Roberts, S. M. Schmidt, A. Bender, and M. R. Frank, *Phys. Rev.* **C60**, 062201 (1999).
  - [17] G. Eichmann, A. Krassnigg, M. Schwinzerl, and R. Alkofer, *Annals Phys.* **323**, 2505 (2008).
  - [18] G. Eichmann, R. Alkofer, I. C. Cloet, A. Krassnigg, and C. D. Roberts, *Phys. Rev.* **C77**, 042202 (2008).
  - [19] G. Eichmann, I. C. Cloet, R. Alkofer, A. Krassnigg, and C. D. Roberts, *Phys. Rev.* **C79**, 012202 (2009).
  - [20] D. Nicmorus, G. Eichmann, A. Krassnigg, and R. Alkofer, *Phys. Rev.* **D80**, 054028 (2009).
  - [21] D. Nicmorus, G. Eichmann, and R. Alkofer, *Phys. Rev.* **D82**, 114017 (2010).
  - [22] G. Eichmann, R. Alkofer, C. S. Fischer, A. Krassnigg, and D. Nicmorus, 1010.0206 [*hep-ph*].
  - [23] D. Nicmorus, G. Eichmann, A. Krassnigg, and R. Alkofer, *Few Body Syst.* **49**, 255 (2011).
  - [24] G. Eichmann, PhD thesis, University of Graz, 0909.0703 [*hep-ph*].
  - [25] G. Eichmann, R. Alkofer, A. Krassnigg, and D. Nicmorus, *Phys. Rev. Lett.* **104**, 201601 (2010).
  - [26] R. Alkofer, G. Eichmann, A. Krassnigg, and D. Nicmorus, *Chin. Phys.* **C34**, 1175 (2010).
  - [27] G. Eichmann, *Phys. Rev.* **D84**, 014014 (2011).
  - [28] H. Sanchis-Alepuz, R. Alkofer, G. Eichmann, and S. Villalba-Chavez, *PoS LC2010*, 018 (2010).
  - [29] R. Delbourgo and M. Scadron, *J.Phys.G* **G6**, 649 (1980).
  - [30] J. Finger, J. Mandula, and J. Weyers, *Phys.Lett.* **B96**, 367 (1980).
  - [31] P. Fomin, V. Gusynin, V. Miransky, and Y. Sitenko, *Riv.Nuovo Cim.* **6N5**, 1 (1983).
  - [32] H. J. Munczek and P. Jain, *Phys.Rev.* **D46**, 438 (1992).
  - [33] H. Munczek, *Phys.Rev.* **D52**, 4736 (1995).
  - [34] P. Maris, C. D. Roberts, and P. C. Tandy, *Phys. Lett.* **B420**, 267 (1998).
  - [35] A. Holl, A. Krassnigg, and C. D. Roberts, *Phys. Rev.* **C70**, 042203 (2004).
  - [36] P. Maris and P. C. Tandy, *Phys. Rev.* **C60**, 055214 (1999).
  - [37] C. Alexandrou *et al.*, *Nucl. Phys.* **A825**, 115 (2009).
  - [38] G. P. Engel, C. B. Lang, M. Limmer, D. Mohler, and A. Schafer (BGR [Bern-Graz-Regensburg]), *Phys. Rev.* **D82**, 034505 (2010).
  - [39] J. M. Zanotti *et al.* (CSSM Lattice), *Phys. Rev.* **D68**, 054506 (2003).
  - [40] C. Gattringer *et al.*, *Phys. Rev.* **D79**, 054501 (2009).
  - [41] C. S. Fischer and R. Williams, *Phys. Rev.* **D78**, 074006 (2008).
  - [42] C. S. Fischer and R. Williams, *Phys. Rev. Lett.* **103**, 122001 (2009).
  - [43] L. Chang and C. D. Roberts, *Phys. Rev. Lett.* **103**, 081601 (2009).
  - [44] L. Chang, Y.-X. Liu, and C. D. Roberts, *Phys.Rev.Lett.* **106**, 072001 (2011).
  - [45] S.-x. Qin, L. Chang, Y.-x. Liu, C. D. Roberts, and D. J. Wilson, 1108.0603 [*nucl-th*].
  - [46] C. R. Allton, W. Armour, D. B. Leinweber, A. W. Thomas, and R. D. Young, *PoS LAT2005*, 049 (2006).
  - [47] V. Mader, G. Eichmann, M. Blank, and A. Krassnigg, *Phys. Rev.* **D84**, 034012 (2011).